Thioamides as Fluorescence Quenching Probes: Minimalist Chromophores to Monitor Protein Dynamics

Jacob M. Goldberg, Solongo Batjargal, & E. James Petersson

Department of Chemistry, University of Pennsylvania
231 South 34th Street, Philadelphia, Pennsylvania 19104-6323 USA.

General Information. Fmoc-L-4-cyanophenylalanine (Fmoc-L-Cnf-OH) was purchased from Peptech (Burlington, MA). Boc-L-thionoleucine-1-(6-nitro)benzotriazolide, Fmoc-L-Gln(Mtt)-OH, and Fmoc-L-Asn(Mtt)-OH were purchased from Bachem (Torrence, CA). 2-chlorotrityl resin, Fmoc-L-Ala-OH, Fmoc-L-Glu(OtBu)-OH, Fmoc-L-Lys(Boc)-OH, Fmoc-L-Leu-OH, Fmoc-L-Arg(Pbf)-OH, Fmoc-L-Pro-OH, Fmoc-L-Thr(tBu)-OH, Fmoc-L-Met-OH, Fmoc-L-Gly-OH, Fmoc-L-Val-OH, Fmoc-L-Phe-OH, Fmoc-L-Asp(OtBu)-OH, and Fmoc-L-Ser(tBu)-OH were purchased from Novabiochem (San Diego, CA). Piperidine and 2-(1*H*-benzotriazol-1-yl)-1,1,3,3-tetramethyluronium hexafluorophosphate (HBTU) were purchased from American Bioanalytical (Natick, MA). Sigmacote, *N*,*N*-diisopropylethylamine (DIPEA), *N*-Boc-1,2,-phenylenediamine, isobutyl chloroformate (IBCF), and L-alanine methyl ester hydrochloride were purchased from Sigma-Aldrich (St. Louis, MO). All other reagents were purchased from Fisher Scientific (Pittsburgh, PA). Milli-Q filtered (18 MΩ) water was used for all solutions (Millipore; Billerica, MA). Matrix-assisted laser desorption ionization (MALDI) mass spectra were collected with a Bruker Ultraflex III MALDI-TOF-TOF mass spectrometer (Billerica, MA). UV absorbance spectra were obtained with a Hewlett-Packard 8452A diode array spectrophotometer. Fluorescence spectra were collected with a Varian Cary Eclipse fluorescence spectrophotometer fitted with a Peltier multicell holder. Circular dichroism experiments were conducted with an Aviv 410 CD spectrometer (Aviv Biomedical; Lakewood, NJ). ^{1}H NMR spectra were collected with Bruker DRX 500 MHz and Bruker DMX 500 MHz

instruments. High-resolution mass spectra were obtained on a Waters LC-TOF mass spectrometer (model LCT-XE Premier) using electrospray ionization in positive mode.

Chemical Synthesis. Route adapted from Shalaby *et al.*[1]

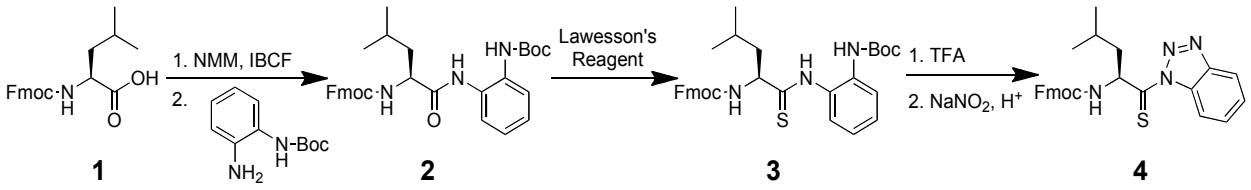

Scheme S1. Synthesis of thioleucine benzotriazolide precursor.

α-*N*-Fmoc-L-leucine-(*N*-Boc)-2-aminoanilide (**2**). Fmoc-Leu-OH (1.7675 g, 5 mmol) was dissolved in 50 mL tetrahydrofuran under argon flow and the solution was cooled to - 10 °C in a 1:3 NaCl: ice bath. *N*-methylmorpholine (NMM, 1.10 mL,10 mmol) and isobutyl chloroformate (0.65 mL, 5 mmol) were added dropwise with stirring. After 15 min, *N*-Boc-1,2-phenylenediamine (1.0483 g, 5 mmol) was added and the reaction was allowed to proceed with stirring under argon flow at - 10 °C for 2 h. The reaction was then allowed to proceed overnight with stirring at room temperature under an argon atmosphere for a total run time of 20 h. The crude reaction mixture was reduced to dryness by rotary evaporation and brought up in 40 mL ethyl acetate (EtOAc). This solution was extracted against 40 mL each of 1 M Na_2HPO_4, brine, 5% $NaHCO_3$, and brine. The combined aqueous solution was extracted once against 100 mL EtOAc. The combined organic mixture was then evaporated to 25 mL and run on a flash column in 13:7 petroleum ether/ethyl acetate. The purified product was evaporated to dryness to afford white foam (2.5157 g, 4.6 mmol, 92% yield). ^{1}H NMR ($CDCl_3$): δ 8.40 (s, 1H), 7.75 (d, J = 7.5 Hz, 2H), 7.59-7.56 (m, 2H), 7.47-7.46 (m, 2H), 7.40-7.36 (m, 2H), 7.30-7.25 (m, 2H), 7.20-7.17 (dt, J = 7.7 Hz, 1H), 7.15-7.12 (dt, J = 7.7 Hz, 1H), 6.79 (s, 1H), 5.30 (br. d, J = 6.2 Hz, 1H), 4.50-4.42 (m, 2H), 4.32 (br. d, J = 5.0 Hz, 1H), 4.23-4.20 (t, J = 6.7 Hz 1H), 1.82-1.71 (br. m, 2H), 1.67-1.60 (br. m, 1H), 1.48 (s, 9H), 0.99 (d, J = 5.4 Hz, 6H). ESI$^+$-MS: calculated for $C_{32}H_{37}N_3O_5Na^+$: 566.2631; found $[M+Na]^+$: 566.2612.

α-*N*-Fmoc-L-thioleucine-(*N*-Boc)-2-aminoanilide (**3**). Lawesson's Reagent (1.462 g, 3.6 mmol) was added to a solution of **2** (2.618 g, 4.82 mmol) in CH_2Cl_2 (50 mL). The reaction was then allowed to stir and reflux at 50 °C under an argon environment for 90 min. Solvent was removed by rotary evaporation and the crude reaction mixture was re-dissolved in a minimal amount of CH_2Cl_2. This solution was run on a silica gel column in 7:3 petroleum ether: ethyl acetate to afford **3** as yellow foam (0.5548 g, 0.99 mmol, 20% yield). Recovered starting material (1.62 g, 2.98 mmol) was refluxed in CH_2Cl_2 (50 mL) at 50 °C with fresh Lawesson's Reagent (0.9041 g, 2.24 mmol) for 2.5 h, and the reaction was purified a second time as described to produce **3** (0.6005 g, 1.07 mmol, 36% yield). The recovered starting material from this reaction (0.9395 g, 1.68 mmol) was re-subjected to a third round of refluxing with fresh Lawesson's Reagent (0.5097 g, 1.26 mmol) for 22.5 h and subsequently purified to give **3** (0.68 g, 1.21 mmol, 72% yield) and un-reacted starting material (0.24 g, 0.44 mmol). In this manner, **3** (1.83g, 3.27 mmol) was produced in 68% overall yield. ^{1}H NMR ($CDCl_3$): δ 9.72 (s, 1H), 7.77-7.74 (m, 2H), 7.60-7.56 (m, 4H), 7.41-7.34 (m, 2H) 7.31-7.27 (m, 3H), 7.16 (dt, J = 7.7 Hz, 1H), 6.75 (s, 1H), 5.59 (s, 1H), 4.62-4.57 (br. m, 1H), 4.48-4.38 (br. m, 2H), 4.22 (t, J = 6.7 Hz, 1H), 1.86-1.75 (br. m, 3H), 1.46 (s, 9H), 1.00 (br. s, 6H). ESI$^+$-MS: calculated for $C_{32}H_{37}N_3O_4SNa^+$: 582.2402; found $[M+Na]^+$: 582.2410.

α-*N*-Fmoc-L-thioleucine-benzotriazolide (**4**). 1.83 g **3** (3.27 mmol) were incubated with 25% TFA in CH_2Cl_2 (40 mL) on ice with stirring for 150 min. The solvent was removed on a vacuum pump with KOH and dry ice/acetone traps. The resulting orange solid was washed twice with 10 mL CH_2Cl_2, which was removed by rotary evaporation. 20 mL glacial acetic acid diluted with 5% H_2O were added to the dry residue and the mixture was cooled to 0 °C on ice. 0.3384 g $NaNO_2$ (4.90 mmol) were added in small portions over 5 min with constant stirring at 0 °C. After 30 min, the reaction was quenched by addition of 75 mL ice water. The resulting precipitate was collected and washed 3x with ice water and was purified on a silica column in 7:3 petroleum ether: ethyl acetate to afford **4** as a yellow solid (0.75 g, 1.6 mmol, 49% yield).

^{1}H NMR ($CDCl_3$): δ 8.80 (d, *J* = 8.4 Hz, 1H), 8.17 (d, *J* = 8.0 Hz, 1H), 7.78-7.75 (d, *J* = 8.0 Hz 2H), 7.73-7.68 (dd (apparent t), *J* = 7.5 Hz, 1H), 7.64-7.61 (dd (apparent t), *J* = 8.5 Hz, 2H), 7.59-7.56 (dd (app. t), *J* = 7.5 Hz, 1H), 7.42-7.39 (dd (apparent t), *J* = 7.5 Hz, 2H), 7.34-7.31 (dd (apparent t), *J* = 7.5 Hz, 2H), 6.38-6.34 (m, 1H), 5.68 (d, *J* = 9.4 Hz, 1H), 4.51-4.48 (m, 1H), 4.42-4.36 (br. m, 1H), 4.24 (t, *J* = 6.8 Hz, 1H), 1.90-1.82 (br. m, 2H), 1.71-1.67 (m, 1H), 1.13 (d, *J* = 6.0 Hz, 3H), 0.96 (d, *J* = 6.0 Hz, 3H). ESI$^+$-MS: calculated for $C_{27}H_{26}N_4O_2SNa^+$: 493.1674; found $[M+Na]^+$: 493.1670.

Peptide Synthesis and Purification. Leu-Pro$_2$-Cnf (LP_2F^*) and Leu'-Pro$_2$-Cnf ($L'P_2F^*$) were synthesized on a 12.5 μmol scale on 2-chlorotrityl resin. For each synthesis, 2-chlorotrityl chloride resin (100-200 mesh; 0.6 mmol substitution/g; 12.5 μmol) was added to a dry glass peptide synthesis reaction vessel (RV), the walls of which had been treated previously with Sigmacote. The resin was swollen by two successive 15 min incubations with 5 mL dimethylformamide (DMF) and magnetic stirring. After swelling, DMF was removed with vacuum suction and Fmoc-L-Cnf-OH was coupled to the resin. Fmoc-L-Cnf-OH in DMF (5 equiv; 42 mM, 1.5 mL) and DIPEA (10 equiv; 22 μL) were added to the RV and the mixture was allowed to react for 30 min with magnetic stirring. Spent solution was removed with vacuum suction and the resin beads were washed thoroughly with DMF. Excess DMF was removed with vacuum suction and the resin beads were deprotected by treatment with 20% piperidine in DMF (5 mL) for 20 min with magnetic stirring. The deprotection solution was drained from the RV and the beads were rinsed extensively with DMF. Subsequent amino acid couplings and deprotections proceeded as described above, with the exception of proline and leucine couplings, for which the Fmoc-protected amino acids were activated with HBTU (5 equiv) prior to addition to each reaction. Boc-L-thionoleucine-1-(6-nitro)benzotriazolide (5 equiv) was used to introduce thioleucine into $L'P_2F^*$. The *N*-terminal Fmoc group was removed from LP_2F^* before the peptide was cleaved from the resin. After the beads were washed extensively with DMF and dried with CH_2Cl_2, peptides were cleaved by successive 60 min and 30 min incubations on a rotisserie with 2.5 mL of a fresh cleavage cocktail of trifluoroacetic acid (TFA), water, and

triisopropylsilane (TIPS) (10:9:1 v/v). After each treatment, the resulting solution was expelled from the RV with nitrogen, reduced to a volume of less than 1 mL by rotary evaporation, and diluted with 6 mL of CH_3CN/H_2O (2:1 v/v).

The peptides were purified by reverse-phase HPLC on a Vydac 218TP C18 semi-prep column (Grace/Vydac; Deerfield, IL) using a linear solvent gradient that ranged from 98% to 60% aqueous phase over 19 min, then to 0% aqueous phase over 5 min, then returning to 98% aqueous phase during a 10 min wash out period. Peptides eluted at approximately 22 min with this method. (Fig. S1a-c) MALDI-MS was used to confirm identites (Table S1). Purified peptides were dried in a vacuum centrifuge (Savant/Thermo Scientific; Rockford, IL).

Polyproline peptides Leu-Pro_n-Cnf (LP_nF^*) and Leu'-Pro_n-Cnf ($L'P_nF^*$), n = 3-11, were each synthesized on a 10 μmol scale using a procedure analogous to that described above for $L'P_2F^*$ or LP_2F^*. These peptides were synthesized from a common pot of resin (100 μmol). After coupling the appropriate number of proline residues, a 10 μmol portion of resin was removed from the RV and transferred to a separate, clean RV for leucine or thioleucine coupling. As the synthesis progressed, reagents were scaled accordingly. Peptide cleavage, purification, and characterization followed that of $L'P_2F^*$ or LP_2F^*.

Acetylated polyproline peptides Ac-$L'P_2F^*$ and Ac-LP_2F^* were synthesized as described for their non-acetylated counterparts except thioleucine was incorporated to Ac-$L'P_2F^*$ by coupling α-*N*-Fmoc-L-thioleucine-benzotriazolide (5 equiv) with HBTU (5 equiv) and DIPEA (10 equiv). Peptides were acetylated with a mixture of acetic anhydride (Ac_2O) and NMM in DMF. After deprotection of the *N*-terminal Fmoc group, resin-bound peptides were treated twice with 5 mL portions of DMF/NMM/Ac_2O (42:3:5 v/v) with constant stirring at room temperature for 10 min. After each reaction, the spent solution was expelled as waste with air flow. The peptides were rinsed 3 times with 4 mL aliquots of DMF with shaking and then thoroughly dried. The resin beads were incubated on a rotisserie for 60 min and for 30 min with 2.5 mL portions of fresh TFA/H_2O/TIPS (38:1:1 v/v). Workup and purification followed the method described for LP_2F^*

and L'P_2F*. Using that method, the peptides had retention times around 24 min for Ac-LP_2F* and 26 min for Ac-L′P_2F*. (Fig. S1e)

The villin headpiece subdomain peptide HP35-F*$_{35}$ (sequence LSDEDFKAVFGMTRSAFA-NLPLFKQQNLKKEKGLF*) and the HP35-L'$_1$F*$_{35}$ derivative were each synthesized on a 100 μmol scale using the same general procedures as those described above. Trp_{23} in the native peptide was replaced with Phe_{23} since Cnf and Trp are a known FRET pair.[2] Briefly, a peptide consisting of residues S2-F*35 was synthesized on a 200 μmol scale on 2-chlorotrityl resin beads with 5 equiv amino acid, 10 equiv DIPEA, and 5 equiv HBTU when needed. Before removal of the Fmoc-group from S2, the resin beads were divided into 2 equal portions and transferred to clean RVs for the final coupling of either Fmoc-L-Leu-OH or Boc-L-thionoleucine-1-(6-nitro)benzotriazolide. After removal of the *N*-terminal Fmoc-group from the HP35-F*$_{35}$ peptide with 20% piperidine, the resin beads were washed with CH_2Cl_2, dried under vacuum, and incubated on a rotisserie twice for 60 min with 5 mL portions of fresh TFA/H_2O/TIPS (38:1:1 v/v). After each incubation period, the cleavage cocktail was expelled from the RV with nitrogen and dried by rotary evaporation. The residue was diluted to 10 mL with CH_3CN/H_2O (3:2 v/v). Crude peptides were purified by reverse-phase HPLC with linear solvent gradients that ramped from 98% to 50% aqueous phase over 24 min, then to 0% aqueous phase over 5 min, followed by a 10 min wash out period, during which the solvent system returned to 95% aqueous phase. Using this method, the HP35-F*$_{35}$ peptide eluted at 28.1 min. The peptide was further purified by additional HPLC with linear solvent gradients that ramped from 95% aqueous phase to 70% aqueous phase over 6 min, then to 50% aqueous phases over 20 min, then to 0% aqueous phase over 5 min, followed by a 10 min wash out period, during which the solvent system returned to 95% aqueous phase. Using this method, the peptide eluted at 21.3 min. (Fig. S1d)

Global deprotection and cleavage from the resin of the HP35-L'$_1$F*$_{35}$ peptide was accomplished by two successive 60 min incubations of the resin beads with 5 mL portions of fresh TFA/H_2O/TIPS (18:1:1 v/v). After each incubation period, the cleavage cocktail was expelled from the RV with nitrogen and reduced in volume by rotary evaporation, and diluted to

20 mL with CH_3CN/H_2O (1:1 v/v). This peptide was purified using the same procedure as that for the HP35-F*$_{35}$ peptide and had retention times of 28.5 min for the first pass and 22.0 min for the second pass. (Fig. S1d) After purification, both peptides were dried and characterized by MALDI-MS. (See Table S1)

(*S*)-methyl 2-((*S*)-2-amino-4-methylpentanethioamido)propanoate (thioleucylalanine ester). A solution of alanine methyl ester in tetrahydrofuran (THF) was prepared by treating L-alanine methyl ester hydrochloride (400 μmol) in 2 mL THF with DIPEA (400 μmol; 70 μL) in a septum-capped, oven-dried vial with magnetic stirring. After cooling this solution to 0 °C and purging with argon, a solution of Boc-L-thionoleucine-1-(6-nitro)benzotriazolide (400 μmol) in 6 mL THF was added dropwise over 5 min with argon flow and magnetic stirring. The mixture was allowed to react on ice for 60 min under argon with constant stirring. After rotary evaporation of the solvent, the product was incubated in TFA/H_2O (1:1 v/v) with shaking for 60 min. The crude reaction mixture was again dried by rotary evaporation, and the remaining residue was diluted with CH_3CN/H_2O (1:10 v/v) and purified by HPLC with linear solvent gradients that ramped from 95% aqueous phase to 70% aqueous phase over 6 min, then to 50% aqueous phases over 20 min, then to 0% aqueous phase over 5 min, followed by a 10 min wash out period, during which the solvent system returned to 95% aqueous phase. Using this method, the peptide eluted at 13.6 min. (Fig. S1d)

Table S1. Calculated and Observed Peptide Masses.

Peptide	Calculated m/z $[M+H]^+$	Observed m/z $[M+H]^+$	Calculated m/z $[M+Na]^+$	Observed m/z $[M+Na]^+$
L'A-OMe	233.132	233.196	255.114	255.151
LP_2F^*	498.271	498.200	520.253	520.169
Ac-LP_2F^*	540.282	——	562.264	562.295
L'P_2F^*	514.248	514.062	536.230	536.028
Ac-L'P_2F^*	556.259	——	578.241	578.201
L'P_3F^*	611.301	611.144	633.283	633.098
L'P_4F^*	708.354	708.200	730.336	730.163
LP_5F^*	789.429	789.381	811.411	811.363
L'P_5F^*	805.407	805.278	827.388	827.225
L'P_6F^*	902.459	902.310	924.441	924.262
L'P_7F^*	999.512	999.401	1021.494	1021.352
L'P_8F^*	1096.565	1096.466	1118.547	1118.406
L'P_9F^*	1193.618	1193.512	1215.600	1215.436
$LP_{10}F^*$	1274.693	1274.578	1296.675	1296.565
L'$P_{10}F^*$	1290.670	1290.548	1312.652	1312.494
L'$P_{11}F^*$	1387.723	1387.607	1409.705	1409.542
HP35-F_{35}*	4043.121	4043.532	4065.103	——
HP35-L'$_1F^*_{35}$	4059.098	4059.506	4081.080	——

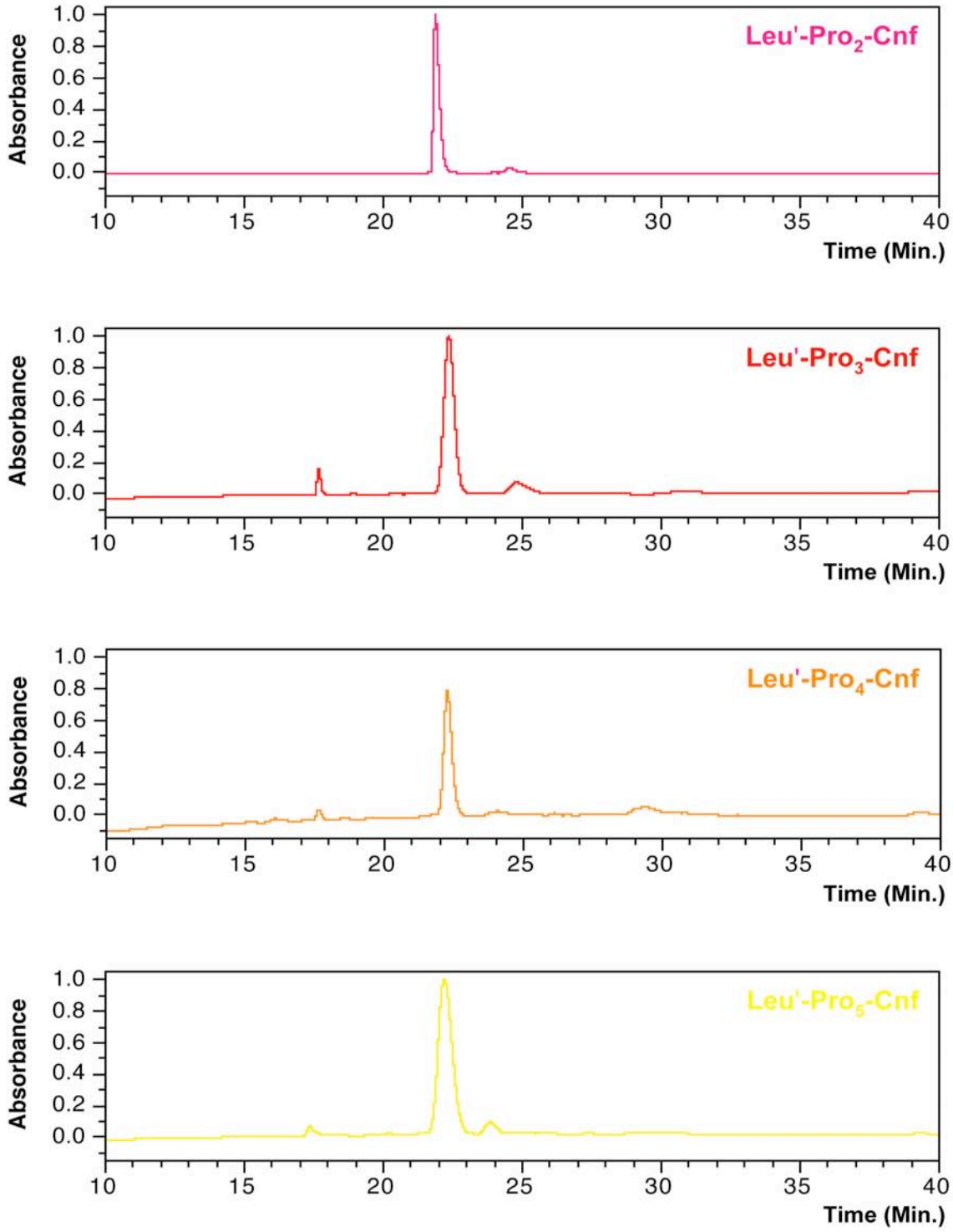

Figure S1a. Analytical HPLC Chromatograms of Purified Peptides. Absorbance at 232 nm (oxoamides) or 277 nm (thioamides) is normalized. Solvent gradients given in text. L'P_nF* peptides colored to match associated UV and fluorescence data.

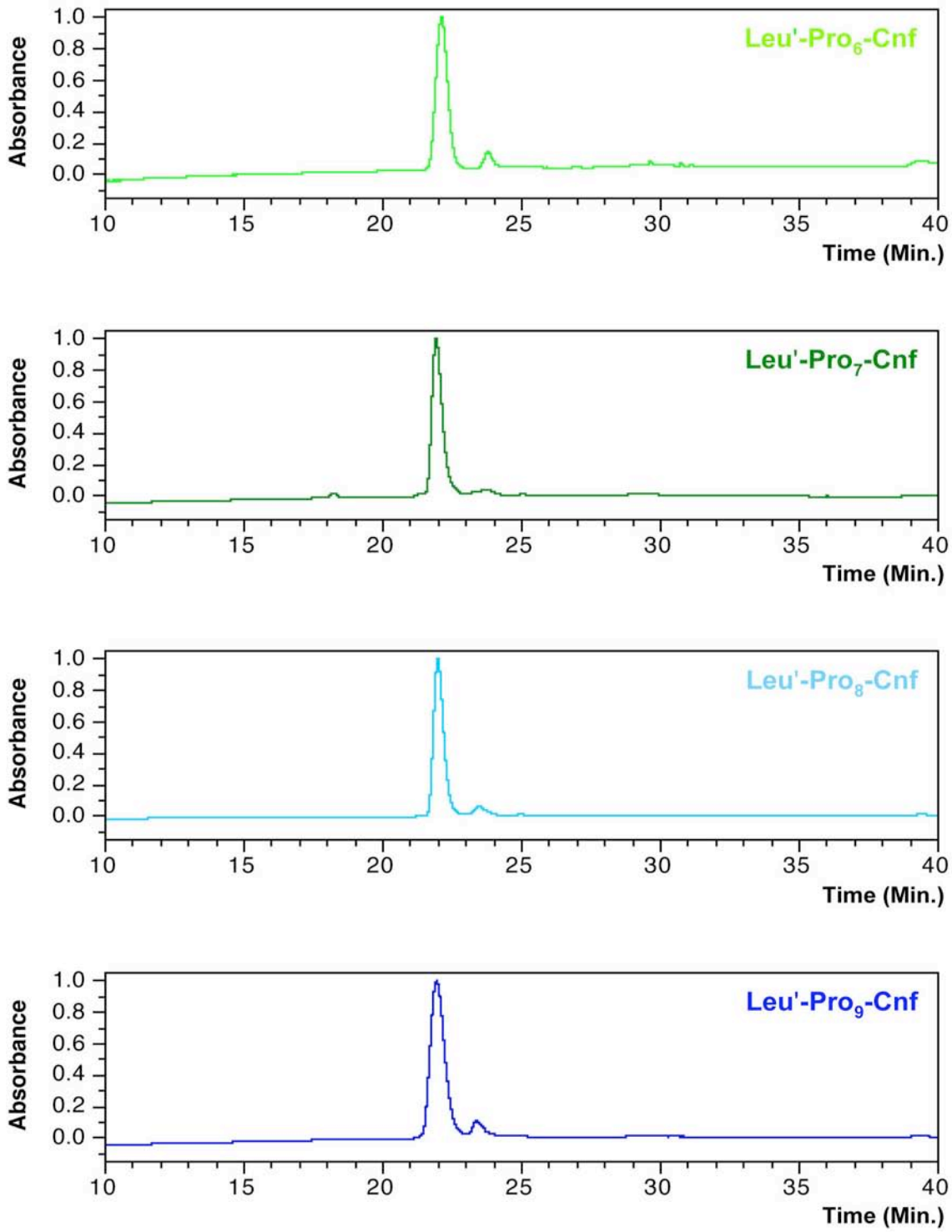

Figure S1b. Analytical HPLC Chromatograms of Purified Peptides. Absorbance at 232 nm (oxoamides) or 277 nm (thioamides) is normalized. Solvent gradients given in text. L'P_nF* peptides colored to match associated UV and fluorescence data.

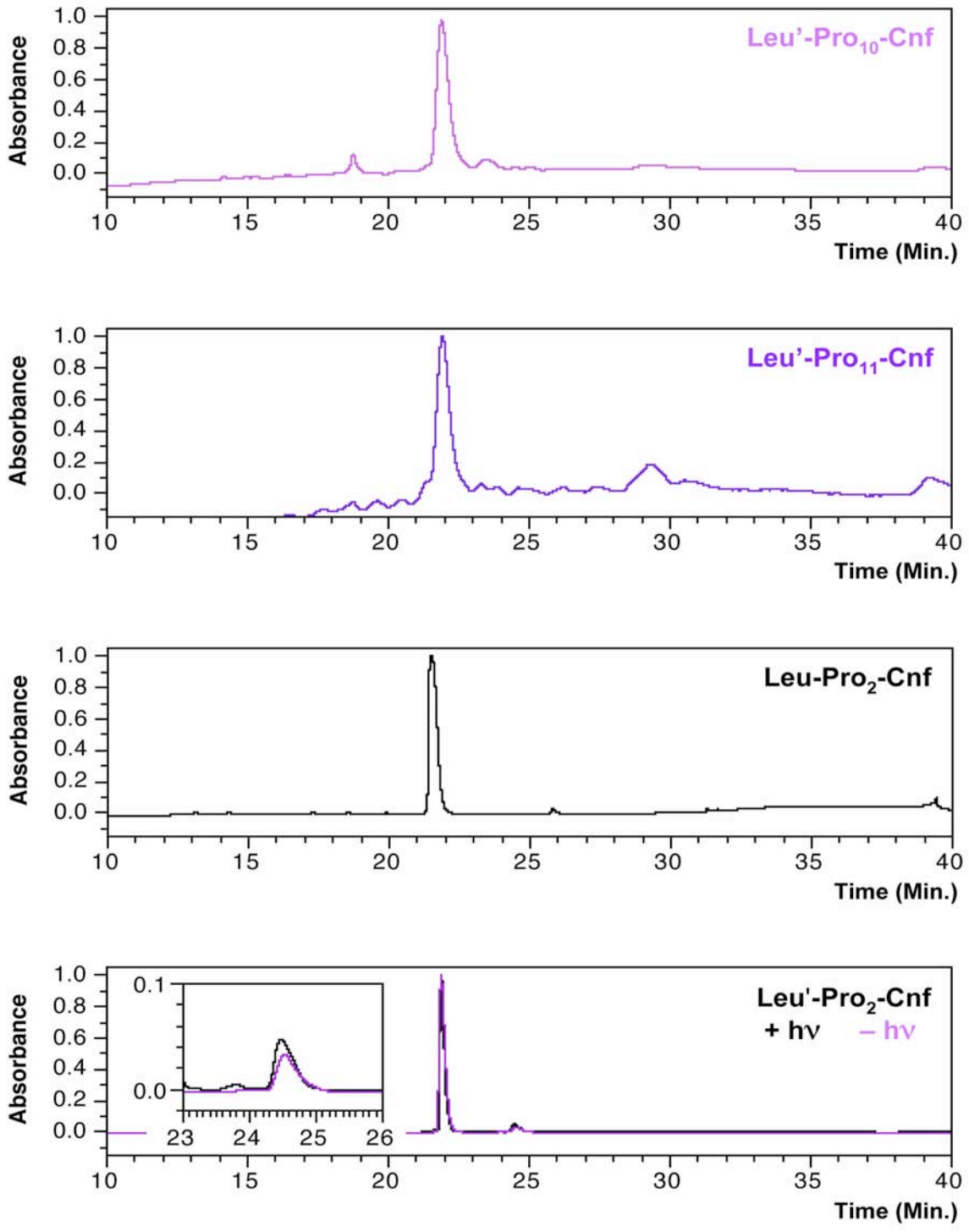

Figure S1c. Analytical HPLC Chromatograms of Purified Peptides. Absorbance at 232 nm (oxoamides) or 277 nm (thioamides) is normalized. Solvent gradients given in text. L'P_nF* peptides colored to match associated UV and fluorescence data. L'P_2F* (+ hν) shown after 1 h of irradiation at 240 nm.

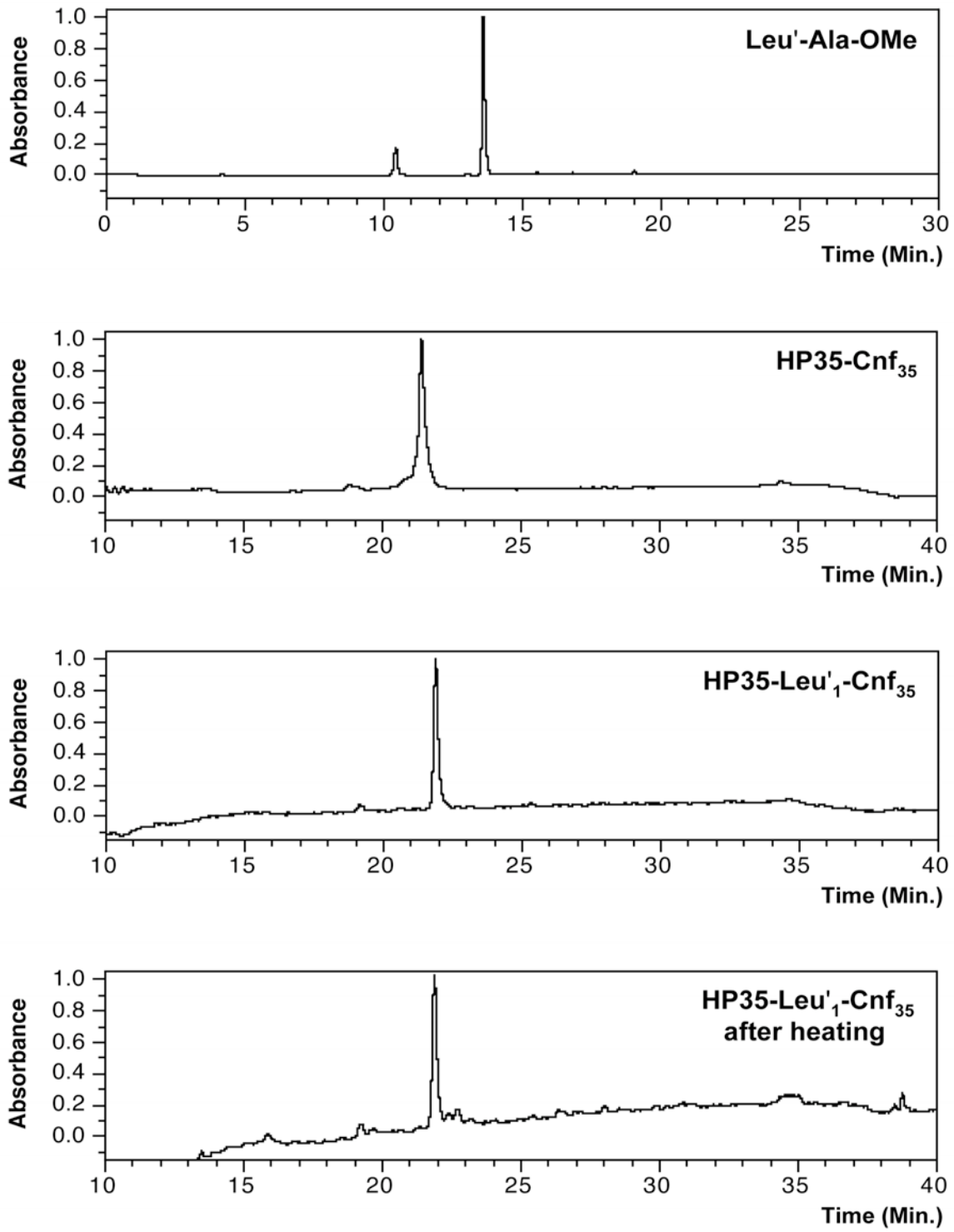

Figure S1d. Analytical HPLC Chromatograms of Purified Peptides. Absorbance at 232 nm (oxoamides) or 277 nm (thioamides) is normalized. Solvent gradients given in text. HP35-Leu'$_1$Cnf$_{35}$ shown after heating to 75 °C in fluorometer.

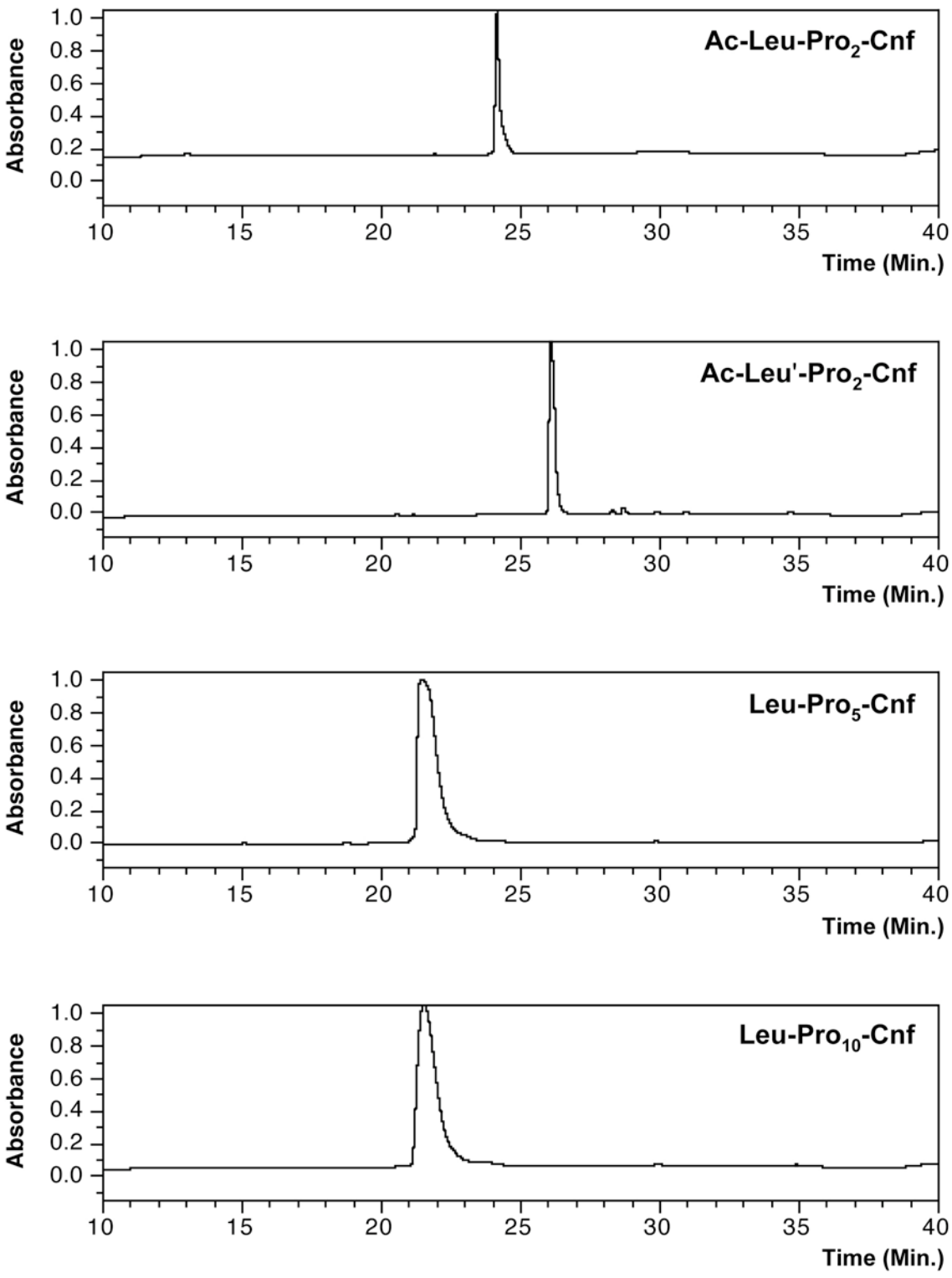

Figure S1e. Analytical HPLC Chromatograms of Purified Peptides. Absorbance at 232 nm (oxoamides) or 277 nm (thioamides) is normalized. Solvent gradients given in text.

Förster Distance Calculation. The Förster distance, R_0, is given in Å by equation (S1)

$$R_0^6 = \frac{9000(\ln 10)\kappa^2 Q_D J}{128\pi^5 n^4 N_A} \quad \text{(S1)}$$

where κ^2 is a geometrical factor that relates the orientation of the donor and acceptor transition moments, Q_D is the quantum yield of the donor, n is the index of refraction of the solvent, N_A is Avogadro's number, and J is the spectral overlap integral defined in units of $M^{-1}\bullet cm^{-1}\bullet nm^4$.[3,4] Combining constants and rearranging gives R_0 as

$$R_0 = 0.211\{Q_D \kappa^2 n^{-4} J\}^{1/6} \quad \text{(S2)}$$

J is formally defined as

$$J = \int_0^\infty f_D(\lambda)\varepsilon_A(\lambda)\lambda^4 d\lambda \quad \text{(S3)}$$

where $\varepsilon_A(\lambda)$ is the molar extinction coefficient of the acceptor at each wavelength λ and $f_D(\lambda)$ is the normalized donor emission spectrum given by

$$f_D(\lambda) = \frac{F_{D\lambda}(\lambda)}{\int_0^\infty F_{D\lambda}(\lambda) d\lambda} \quad \text{(S4)}$$

where $F_{D\lambda}(\lambda)$ is the fluorescence of the donor at each wavelength λ. Fluorescence spectra of LP_2F^* in water were integrated with KaleidaGraph (Synergy Software; Reading, PA) from 270 to 400 nm to calculate $f_D(\lambda)$. UV-Vis spectra of thioleucylalanine ester in water were used to determine $\varepsilon_A(\lambda)$. The literature value of $\varepsilon_{273} = 12{,}400\ M^{-1}\bullet cm^{-1}$ was used to prepare solutions of known concentration.[5] Using values from 3 independent trials, J was calculated to be $7.0 \times 10^{12} \pm 2 \times 10^{11}\ M^{-1}\bullet cm^{-1}\bullet nm^4$. Substituting this result into equation (S1), as well as 0.11 for the quantum yield of Cnf,[6] 1.33 for the index of refraction of water, and 2/3 for κ^2 gives the Förster distance of 15.6 Å for the thioamide-Cnf FRET pair.

Fluorescence Spectroscopy. Dry proline series peptides were brought up in a minimal volume of water or pH 7.0 phosphate buffer (PBS: 150 mM NaCl, 10 mM Na_2HPO_4, pH adjusted with HCl) and then diluted to concentrations of approximately 12 μM, as determined by absorbance at 273 nm (ε_{273} = 13,250 M^{-1}•cm^{-1}) for thioamide-containing peptides or at 232 nm (ε_{232} = 17,700 M^{-1}•cm^{-1}) for LP_2F^* or Ac-LP_2F^*.[2,5] Corrected fluorescence spectra were collected at 25 °C in triplicate for each peptide using quartz fluorometer cells with path lengths of 1.00 cm. For all experiments, the excitation wavelength was 240 nm and emission data was collected from 260 - 400 nm as the average of three scans. The excitation and emission slit widths were 2.5 nm, the scan rate 30 nm/min, the averaging time 1 s, and the data interval 0.5 nm. Examples of fluorescence spectra and associated UV spectra are shown in Figure S2.

Temperature-dependent fluorescence experiments on the villin peptides were conducted in 1.00 cm quartz cells. Peptide concentrations were approximately 5-10 μM as determined by absorbance at 273 nm. The excitation wavelength was 240 nm and emission was monitored at 293 nm. The excitation and emission slit widths were both 5 nm and the averaging time was 1 s. The temperature was held at 5 °C for 5 min, before ramping to 75 °C (HP35-$L'_1F^*_{35}$) or 95 °C (HP35-F^*_{35}) at a rate of 1 °C/min. Temperature-dependent fluorescence data are shown in Figure S13.

To determine the effect of thermal heating and irradiation, samples were analyzed by analytical HPLC before and after irradiation using the method described above. These chromatograms showed little change (Fig. S1d). When HP35-$L'_1F^*_{35}$ was heated to 95 °C, we observed some additional peaks in the HPLC and MALDI-MS (data not shown).

Proline Series Fluorescence. Fluorescence spectra were collected for 12 μM solutions of the L'P_nF* (n = 2 - 10 or 11) series peptides and for LP_2F* as described above.

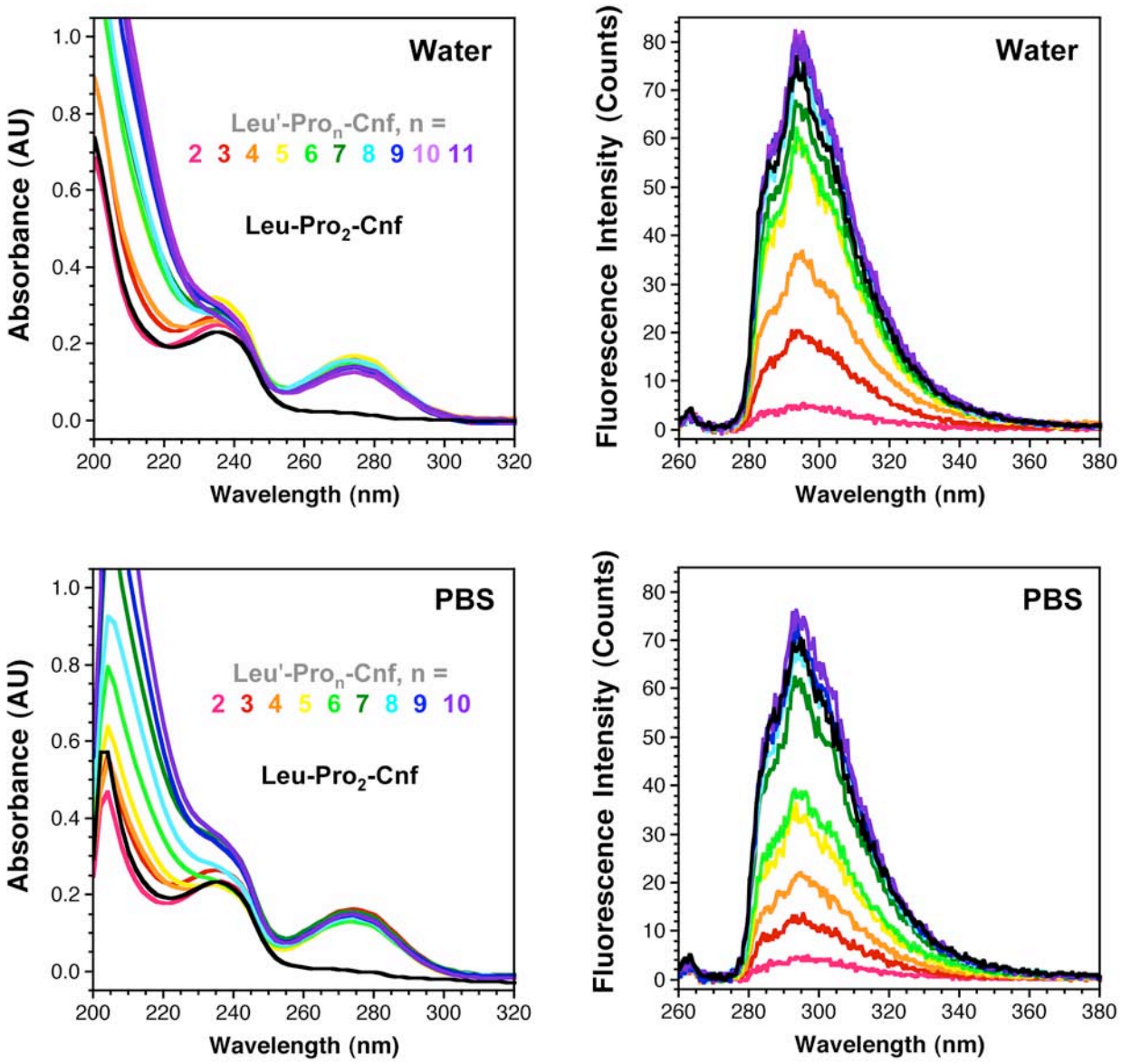

Figure S2. UV Absorption and Fluorescence Spectra for Pro Series in Water or pH 7 Phosphate Buffer. Left: UV spectra collected between 200 and 320 nm and background corrected to against absorption at 500 nm. Right: Fluorescence emission spectra collected between 260 and 380 nm with excitation at 240 nm. Emission spectra colored according to corresponding absorption spectrum.

The intensity at 293 nm was averaged from three trials for each peptide and this was plotted against the number of prolines in the peptide. (Fig. S3) These data were fit to the equation (S5)

using Kaleidagraph, where F_0 was adjustable and R_0 was fixed at 15.6 Å (~ 5.1 prolines, see Molecular Dynamics section below). For data taken in phosphate buffer, a value of 69.9 counts was obtained for F_0.

$$F = F_0 \left\{ 1 - \frac{1}{1 + \left(\frac{R}{R_0}\right)^6} \right\} \qquad \text{(S5)}$$

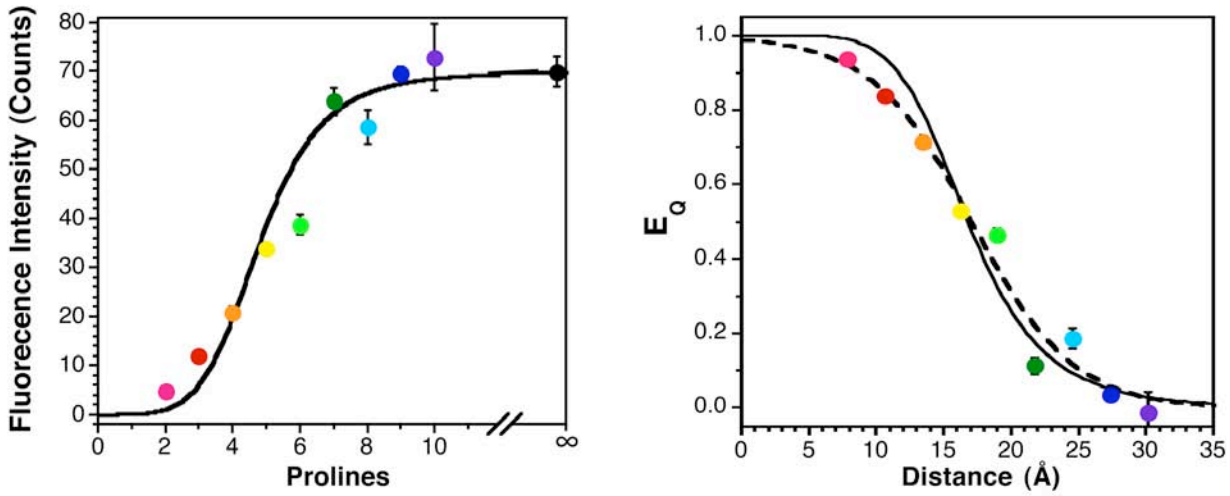

Figure S3. Proline Series Fluorescence Data in PBS. Left: The fluorescence emission at 293 nm of Leu'-Pro_n-Cnf (n = 2 - 10) is shown (3 trials per peptide, bars represent standard error). The "∞" data point indicates the fluorescence of Leu-Pro_2-Cnf. The solid line indicates the distance dependence predicted by Förster theory with R_0 = 15.6 Å (~ 5.1 prolines). Right: Fluorescence intensities converted to E_Q and fit to a $1/R^6$ (solid trace) or $1/e^R$ (dashed trace) distance dependence as described. For both plots, colors match primary data in Figure S2.

Fluorescence intensities were then converted to E_Q according to equation (S6)

$$E_Q = 1 - (F/F_0) \qquad \text{(S6)}$$

and plotted against the computed chromophore separation for each peptide (obtained from MD simulations, see below). These data were fit to equation (S7) using Kaleidagraph, where R_0 is an adjustable parameter. An R_0 value of 16.5 Å was obtained, with a goodness-of-fit (r^2) of 0.973.

$$E_Q = \frac{1}{1 + \left(\frac{R}{R_0}\right)^6} \qquad \text{(S7)}$$

A Dexter energy transfer mechanism was also considered.[7] We tested fitting the E_Q data to a $1/e^R$ distance dependence according to equation (S8), where L_{Dex} (considered to be the sum of the chromophore radii) and k are adjustable.[8] The Dexter fit with L_{Dex} = 7.1 Å and k = 8.9 x 10^{-3} is superior (r^2 = 0.986) to the Förster fit. The sum of the Cnf and thioamide radii ($R_{Cnf} + R_{SCN}$) determined from quantum mechanical calculations is 7.6 Å (see below).

$$E_Q = \frac{1}{1 + ke^{2R/L_{Dex}}} \qquad \text{(S8)}$$

Data taken in PBS are reported in the main text. A comparable distance dependence was seen for data taken in pure water, with a value of 78 counts F_0 obtained by fitting to equation (S5).

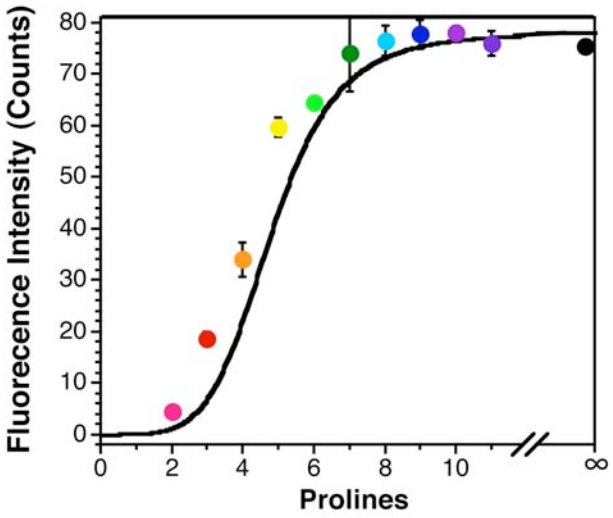

Figure S4. Proline Series Fluorescence Data in Water. The fluorescence emission at 293 nm of Leu'-Pro_n-Cnf (n = 2 - 11) is shown (3 trials per peptide, bars represent standard error). The "∞" data point indicates the fluorescence of Leu-Pro_2-Cnf. The solid line indicates the distance dependence predicted by Förster theory with R_0 = 15.6 Å (~ 5.1 prolines). Colors match primary data in Figure S2

Solvent Effects on E_Q. A recent report by Carrico, Raleigh, and coworkers has shown that the *N*-terminal amine can quench Cnf fluorescence in its deprotonated form.[9] We compared fluorescence emission from equimolar solutions of LP_2F^*, $L'P_2F^*$, and their acetylated forms in phosphate buffer, pH 7.0. As there is no difference in the emission spectra of the free and acetylated forms of the peptides (Fig. S5), we conclude that the *N*-terminal amine does not significantly quench Cnf in LP_2F^* or $L'P_2F^*$ at pH 7.0. Therefore, there is no need to deconvolute an *N*-terminal amine effect from thioamide quenching of Cnf.

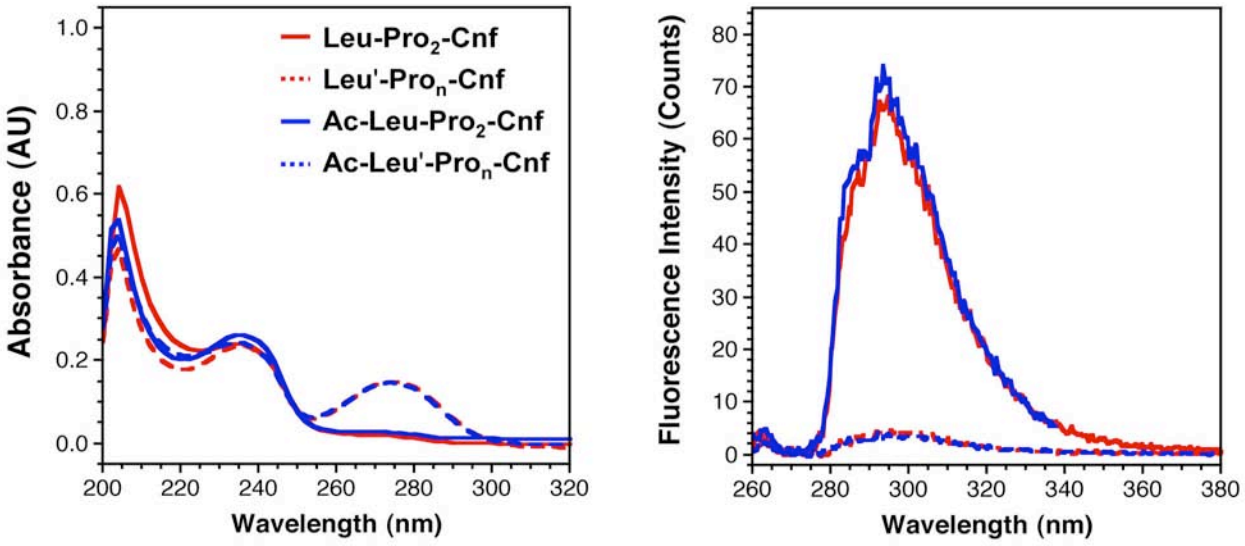

Figure S5. Amine Quenching Studies. Left: UV/Vis spectra of LP_2F^*, $L'P_2F^*$, Ac-LP_2F^*, and Ac-$L'P_2F^*$ in phosphate buffer, pH 7.0 collected between 200 and 320 nm and background corrected to against absorption at 500 nm. Right: Fluorescence emission spectra of the same solutions collected between 260 and 380 nm with excitation at 240 nm.

Thioamide Isomerization. Like oxoamides, thioamides are found primarily in the *trans* form, though in different proportions.[10] Both types of amides can be isomerized to the *cis* form by irradiation; thioamides require 250 - 280 nm ($\pi \rightarrow \pi^*$) or 320 - 400 nm ($n \rightarrow \pi^*$) light.[5] Thus, if Cnf quenching occurs by FRET, one might expect that stimulation of the thioamide to electronically excited states would result in *cis*/*trans* isomerization. In order to determine the effects of irradiation and subsequent Cnf fluorescence quenching on the most efficient (highest

E_Q) of our proline series peptides L'P_2F*, we performed one hour fluorometer experiments followed by either immediate injection onto the HPLC, UV/Vis spectroscopy, or circular dichroism (CD) spectroscopy. During the hour long irradiation, no change in fluorescence was observed (data not shown). The HPLC injection indicates a small increase from 7% to 9% *cis* by LC area (Fig. S1c Bottom). UV/Vis spectra taken before and 30 s after fluorometer irradiation show a less than 0.2% change (Fig. S6 Left). Difference spectra (Pre – Post) in fact show a decrease at 275 nm and an increase at 290 nm, which would be indicative of increased *trans*, not *cis* isomer, as the *cis* isomer is red-shifted relative to the *trans*. CD spectra obtained before and (5 to 15 min) after flourometer experiments show a small change that would also be indicative of increased *trans* isomer, not *cis* (Fig. S6 Right).

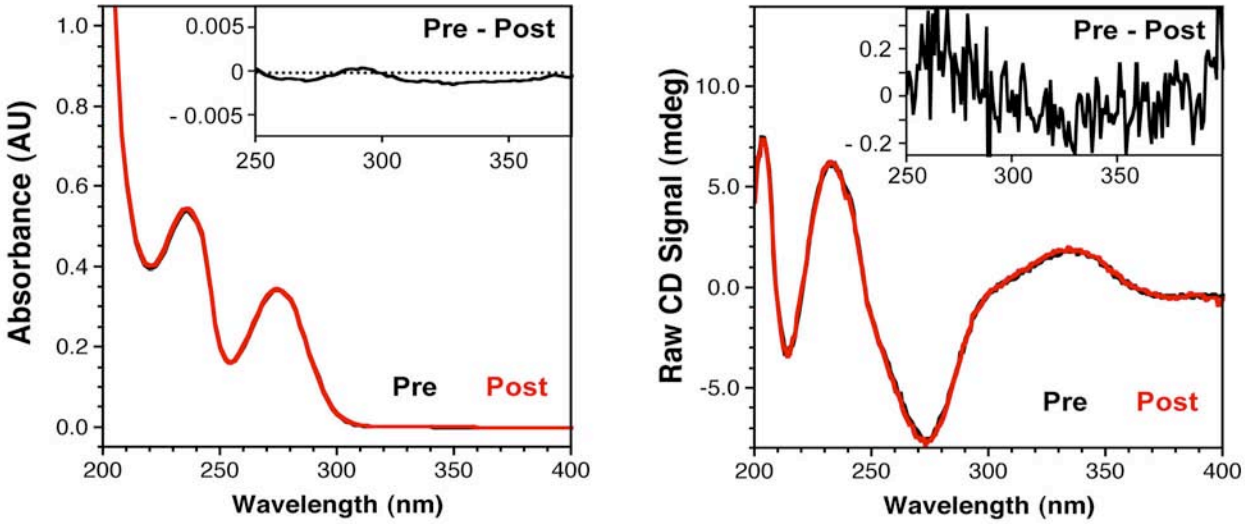

Figure S6. Thioamide Isomerization Studies. Left: UV/Vis spectra of L'P_2F* obtained before and after 1 h of fluorometer irradiation at 240 nm. Inset shows difference spectrum (preirradiation – post irradiation). A 1% change in the absorption spectrum would be ± 0.0035 AU. Right: CD spectra of L'P_2F* obtained before and after 1 h of fluorometer irradiation at 240 nm. Inset shows difference spectrum (preirradiation – post irradiation). Wavelength-dependent CD spectra were obtained in water at 25 ºC in continuous scan mode with a 1 nm data pitch, 30 nm/min scanning speed, 5 s averaging time, and 1 nm band width.

Given that the sample was stirred continuously during irradiation, reported quantum yields for thioamide *trans*-to-*cis* isomerization are 10 to 40%, and the thermal isomerization back to the *trans* form is reported to be slow ($t_{1/2} \geq 10$ min), one could reasonably expect to see significant *cis* isomer present, particularly in the UV/Vis spectra obtained just 30 s after fluorometer irradiation ceased. Thus, these data imply that steady-state isomerization levels during fluorescence experiments are negligible, at best. As noted in the main text, this is seemingly inconsistent with the FRET mechanism expected from the Cnf/thioamide spectral overlap and will be investigated further.

Quantum Mechanical Calculations. Benzonitrile and thioformamide structures were optimized at the B3LYP level of theory with an aug-cc-pVTZ basis set using GAUSSIAN 03 (Gaussian, Inc.; Wallingford, CT).[11] CIS(D) single point energies were then calculated with an aug-cc-pVTZ basis set to identify the transition dipole moments for FRET fitting and the molecular orbitals involved in the spectroscopically relevant transitions. Specifically, for benzonitrile, we analyzed excited state 1, which has an excitation energy of 5.119 eV, corresponding to an absorption at 242 nm. The dominant transitions for this excited state are: 1) from occupied molecular orbital (MO) 26 to unoccupied MO 33, which is a transition from a delocalized ring π bonding orbital to a ring/nitrile π* antibonding orbital, and 2) from occupied molecular orbital (MO) 27 to unoccupied MO 36, which is a transition from a ring/nitrile π bonding orbital to a delocalized ring π* antibonding orbital. The ground to excited state transition dipole moment associated with excited state 1 is perpendicular to the major axis of benzonitrile and in the plane of the molecule, in good accord with previous results.[12,13] (Fig. S7) For Dexter fitting, the benzonitrile diameter (d_{Cnf} = 8.58 Å) was computed as the sum of the N1

to C8 distance (5.33 Å) plus the van der Waals radii of nitrogen (1.55 Å) and carbon (1.70 Å).[14] The van der Waals radius (R_{Cnf} = 4.29 Å) was computed as one half of this value.

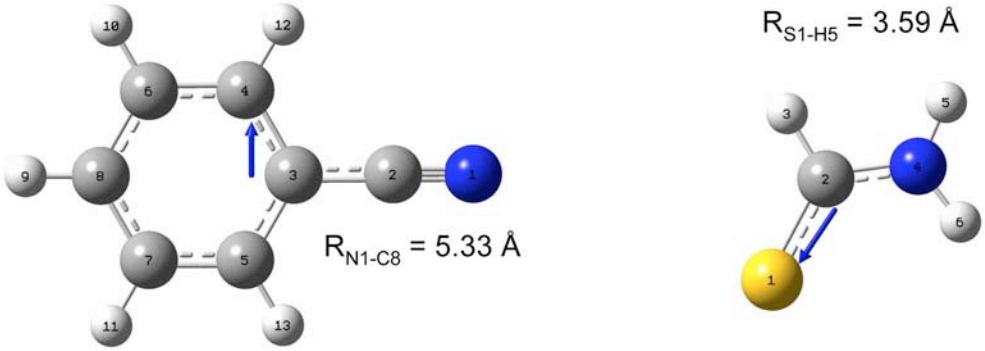

Figure S7. Transition Dipoles of Benzonitrile and Thioformamide. CIS(D)/aug-cc-pVTZ calculated electronic transition dipole moments for first excited state of benzonitrile (left) and second excited state of thioformamide (right) using B3LYP/aug-cc-pVTZ optimized geometries. Arbitrary vector scaling was chosen for clarity. Figure rendered using Gaussview 4.1. (Gaussian, Inc.; Wallingford, CT)

For thioformamide, we analyzed excited state 2, which has an excitation energy of 4.980 eV, corresponding to an absorption at 249 nm. The dominant transition for this excited state is one from occupied MO 15 to unoccupied MO 21, a transition from a C=S π bonding orbital to π* antibonding orbital delocalized over the entire molecule. The transition dipole moment associated with excited state 2 is in the plane of the molecule and runs from the midpoint of the C-N bond toward the S atom. (Fig. S7) Again, this is in good accord with previous results.[5] For Dexter fitting, the thioamide diameter (d_{SCN} = 6.94 Å) was computed one half of the sum of the S1 to H5 distance (3.59 Å) plus the van der Waals radii of sulfur (1.80 Å) and carbon (1.55 Å).[14] The van der Waals radius (R_{SCN} = 3.47 Å) was computed as one half of this value.

Calculated geometries, excitation energies, MO descriptions, and transition dipole vectors for the transitions for both molecules are included on the following pages.

Benzonitrile

Center Number	Atomic Number	Atomic Type	Coordinates (Angstroms) X	Y	Z
1	7	0	0.000000	0.000000	3.191106
2	6	0	0.000000	0.000000	2.038716
3	6	0	0.000000	0.000000	0.608377
4	6	0	0.000000	1.211768	-0.090654
5	6	0	0.000000	-1.211768	-0.090654
6	6	0	0.000000	1.205504	-1.477425
7	6	0	0.000000	-1.205504	-1.477425
8	6	0	0.000000	0.000000	-2.171581
9	1	0	0.000000	0.000000	-3.252972
10	1	0	0.000000	2.142394	-2.016942
11	1	0	0.000000	-2.142394	-2.016942
12	1	0	0.000000	2.143489	0.456490
13	1	0	0.000000	-2.143489	0.456490

Ground to excited state transition electric dipole moments (Au):

State	X	Y	Z	Dip. S.	Osc.
1	0.0000	0.3305	0.0000	0.1092	0.0157
2	0.0000	0.0000	-0.8872	0.7871	0.1135
3	0.0000	0.0000	0.0000	0.0000	0.0000
4	-0.2599	0.0000	0.0000	0.0676	0.0116

Excitation energies and oscillator strengths:

```
Excited State 1: Singlet-B2     5.8704 eV  211.20 nm  f=0.0157
        26 -> 33         0.49396
        26 -> 34        -0.18769
        26 -> 40        -0.10958
        27 -> 36        -0.39675
        27 -> 51        -0.16025
Excited State 2: Singlet-A1     5.8877 eV  210.58 nm  f=0.1135
        26 -> 36         0.33356
        26 -> 51         0.13475
        27 -> 33         0.51780
        27 -> 34        -0.20499
        27 -> 40        -0.10005

**********************************************************************
 CIS(D) Correction to the CiSingles state  1
**********************************************************************
 CIS    Exc. E:  0.215732732534     a.u.     5.87039 eV   211.20278 nm
 CIS(D) doubles : -0.170249969451
 CIS(D) triples :  0.142631106362
 CIS(D) Total   : -0.276188630892E-01        E(CIS(D))=  -323.646774071
 CIS(D) Exc. E:  0.188113869445     a.u.     5.11884 eV   242.21155 nm

**********************************************************************
 CIS(D) Correction to the CiSingles state  2
**********************************************************************
 CIS    Exc. E:  0.216367980630     a.u.     5.88767 eV   210.58270 nm
 CIS(D) doubles : -0.127116626341
 CIS(D) triples :  0.140748369438
 CIS(D) Total   :  0.136317430975E-01        E(CIS(D))=  -323.604888216
 CIS(D) Exc. E:  0.229999723728     a.u.     6.25861 eV   198.10177 nm
```

Thioformamide

Center Number	Atomic Number	Atomic Type	Coordinates (Angstroms) X	Y	Z
1	8	0	1.196487	0.233372	0.000000
2	6	0	0.000000	0.418862	0.000000
3	1	0	-0.446302	1.428411	0.000000
4	7	0	-0.937316	-0.562333	0.000000
5	1	0	-1.917656	-0.346137	0.000000
6	1	0	-0.646722	-1.526088	0.000000

Ground to excited state transition electric dipole moments (Au):

state	X	Y	Z	Dip. S.	Osc.
1	0.0000	0.0000	0.0358	0.0013	0.0001
2	-0.6848	-1.0571	0.0000	1.5864	0.2227

CIS Excitation energies and oscillator strengths:

```
Excited State   1:   Singlet-A"     4.1161 eV  301.22 nm  f=0.0001
      16 -> 21          .62427
      16 -> 22         -.11568
      16 -> 29         -.27856
Excited State   2:   Singlet-A'     5.7288 eV  216.42nm  f=0.2227
      15 -> 21          .58536
      15 -> 22         -.15900
      15 -> 29         -.18639
      16 -> 17          .18505
      16 -> 23         -.10027
```

```
**********************************************************************
 CIS(D) Correction to the CiSingles state  1
**********************************************************************
 CIS    Exc. E:  0.151264621875     a.u.     4.11612 eV   301.21619 nm
 CIS(D) doubles : -0.128969646899
 CIS(D) triples :  0.101032871126
 CIS(D) Total   : -0.279367757723E-01        E(CIS(D))=  -492.075343331
 CIS(D) Exc. E:  0.123327846103     a.u.     3.35592 eV   369.44903 nm

**********************************************************************
 CIS(D) Correction to the CiSingles state  2
**********************************************************************
 CIS    Exc. E:  0.210529948830     a.u.     5.72881 eV   216.42219 nm
 CIS(D) doubles : -0.126765686363
 CIS(D) triples :  0.992513179135E-01
 CIS(D) Total   : -0.275143684496E-01        E(CIS(D))=  -492.015655597
 CIS(D) Exc. E:  0.183015580380     a.u.     4.98011 eV   248.95887 nm
```

Molecular Dynamics Calculations: Polyprolines. Starting geometries for nine proline series peptides (with *N*-terminal Leu, *C*-terminal Phe and n intervening prolines, with n = 2-10) were generated using polyproline type II helix ϕ and ψ angles of - 78° and 149°, respectively. All peptide bonds were initially *trans* (i.e. ω = 180°). *N*- and *C*- termini were left as charged amines and carboxylates, respectively. These were inserted into a TIP3P water box with 10 Å periodic boundaries and no ions. Simulations were performed using the NAMD 2.7b2 package and the CHARMM27 all-atom force field.[15] Covalent bonds involving hydrogen were held rigid using the SHAKE algorithm, allowing a 2 fs time step. A cutoff distance of 12 Å was maintained in calculating nonbonded interactions. Bonded and nonbonded forces were evaluated at every time step, and full electrostatic forces were evaluated at every other time step through application of the particlemesh Ewald (PME) method.[16] The simulation was initiated at 100 K, equilibrated for 25 ps, and warmed to 300 K at a rate of 0.025 K/fs. After warmup, 5 x 10^6 step trajectories (10 ns) were run in the constant temperature and pressure (NPT) ensemble at 300 K.

Chromophore Geometries: Polyprolines. For each 10 ns trajectory, a Tcl script was run in VMD (http://www.ks.uiuc.edu/) to cull distance and orientation information for the leucyl carbonyl and phenylanine ring at every tenth timestep over the last 9 ns of the trajectory. Transition dipole vectors were determined from the geometries in accordance with the vectors identified in the quantum mechanical calculations described above. The script identified the midpoint between CE1 and CE2 (CEmp) of Phe as a proxy for the center of the Cnf transition dipole. Likewise, the script identified the midpoint between Leu_1 C and Pro_2 N (CNmp) as a proxy for the midpoint of the thioamide dipole. The interchromophore distance (*R*) was determined as the distance between these two midpoints. This distance, assigned to each proline series peptide, was used in fits to both Förster and Dexter mechanisms.

The MD data set was also used to calculate theoretical FRET efficiencies for each peptide. The donor-acceptor dihedral angle (ϕ_{DA}) was determined as the Leu O, CNmp, CEmp, Phe CE2 dihedral angle. The donor angle (θ_D) was determined as the CNmp, CEmp, CE2 angle; and acceptor angle (θ_A) was determined as the Leu O, CNmp, CEmp angle. These parameters are illustrated in Figure S8.

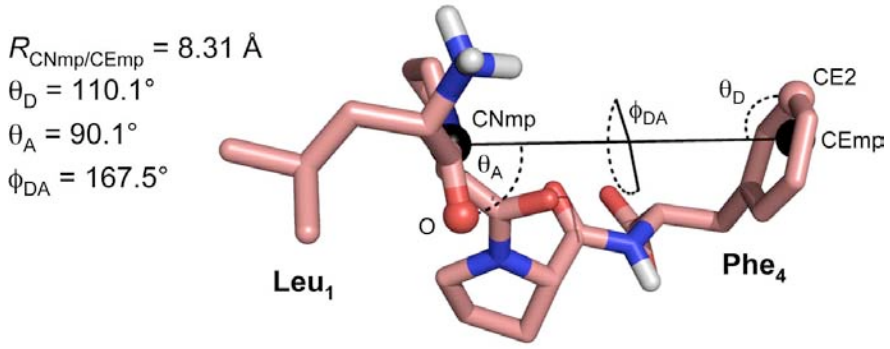

Figure S8. FRET Orientational Parameters. Timestep 215 from Leu-Pro$_2$-Phe simulation shown with atoms used in determining κ^2 and relevant distances and angles illustrated. CNmp and CEmp indicated by black spheres. Figure rendered using PyMOL. (DeLano Scientific, LLC; South San Francisco, CA)

The orientational parameter from Förster theory, κ^2, was calculated as:

$$\kappa^2 = (\sin\theta_D \sin\theta_A \cos\phi_{DA} - 2\cos\theta_D \cos\theta_A)^2 \qquad \text{(S9)}$$

where ϕ_{DA}, θ_D, and θ_A are defined as above.[4] Instantaneous R_0 values were calculated using equations (S2) and (S3) where the donor quantum yield (Q_D) is taken as 0.11,[6] the spectral overlap integral (J) is calculated as above, and the index of refraction (n) is taken as 1.33. For each timestep, this value of R_0 was used to calculate an instantaneous FRET efficiency (E_{FRET}) using the corresponding donor-acceptor separation, R (the CNmp/CEmp distance). Efficiency was calculated using equation (S7). Time averaged values for R, κ^2, R_0, and E_{FRET} are collected in Table S2 for the members of the proline series.

Table S2. Orientational Parameters and Theoretical E_{FRET} Determined from MD Simulations[a]

Leu-Pro$_2$-Phe	R	κ^2	R_0	E_{FRET}
Average	7.8	1.14	15.3	0.92
RMSD	1.1	1.09	3.9	0.18
Leu-Pro$_3$-Phe	R	κ^2	R_0	E_{FRET}
Average	10.3	1.08	15.1	0.79
RMSD	1.9	1.07	4.0	0.28
Leu-Pro$_4$-Phe	R	κ^2	R_0	E_{FRET}
Average	13.2	1.13	15.3	0.64
RMSD	1.4	1.08	3.9	0.30
Leu-Pro$_5$-Phe	R	κ^2	R_0	E_{FRET}
Average	15.7	1.10	15.0	0.46
RMSD	1.8	1.13	4.1	0.30
Leu-Pro$_6$-Phe	R	κ^2	R_0	E_{FRET}
Average	19.6	1.16	15.4	0.26
RMSD	2.2	1.10	4.0	0.21
Leu-Pro$_7$-Phe	R	κ^2	R_0	E_{FRET}
Average	22.0	1.18	15.5	0.17
RMSD	1.7	1.10	3.9	0.15
Leu-Pro$_8$-Phe	R	κ^2	R_0	E_{FRET}
Average	24.7	1.12	15.0	0.10
RMSD	2.1	1.12	4.3	0.10
Leu-Pro$_9$-Phe	R	κ^2	R_0	E_{FRET}
Average	27.0	1.20	15.5	0.06
RMSD	1.4	1.15	4.0	0.06
Leu-Pro$_{10}$-Phe	R	κ^2	R_0	E_{FRET}
Average	30.1	1.06	15.0	0.03
RMSD	2.4	1.06	4.1	0.04

[a] Parameters calculated as described in Supporting Information text. All distances in Å.

Comparison of E_{FRET} from MD and E_Q from Experiment. For the proline series, the observed quenching data deviate noticeably from the curve predicted based on Cnf/thioamide spectral overlap (i.e. equation S7 with R_0 = 15.6 Å). In order to determine whether this discrepancy arises from the assumption that chromophore orientations are random (i.e. $\kappa^2 = 2/3$), we compared the time-averaged FRET efficiencies from MD simulations, for which κ^2 is independently determined for each timestep, to the experimental data. Figure S9 shows the calculated FRET efficiencies (from Table S2) and observed quenching efficiencies. While there is reasonable overall agreement, there is still a clear deviation from the 1:1 correlation indicated by the dotted line, which implies that chromophore orientation is not responsible for the deviation from ideal FRET distance dependence.

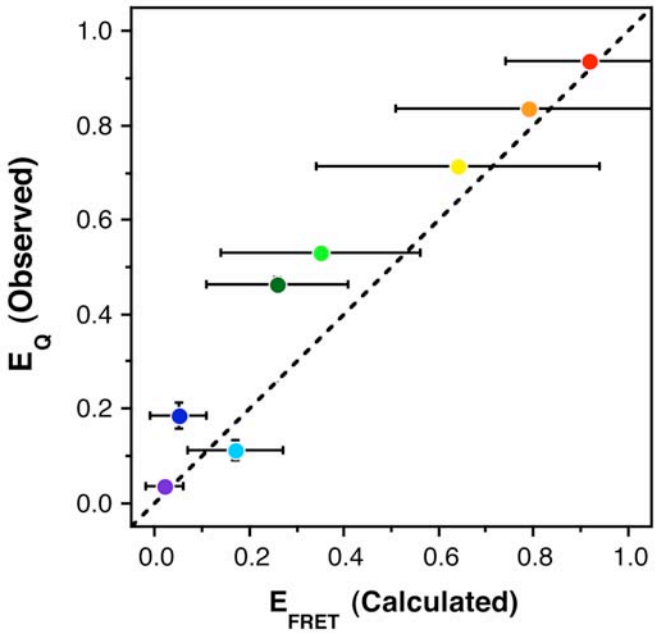

Figure S9. Comparison of Calculated and Observed FRET Quenching Efficiencies. Error bars indicate standard deviation for observed values and RMSD for calculated values. Data points for L'P_nF* colored as in Figs. S2 and S3.

Molecular Dynamics Calculations: HP35. The starting geometry for a simulation of the villin headpiece protein HP35 was taken from PDB structure 1VII.[17] The structure was inserted into a TIP3P water box with 10 Å periodic boundaries and no ions. As with the proline series, simulations were performed using NAMD 2.7b2 with CHARMM27, using the SHAKE algorithm, a 2 fs time step, and a 12 Å nonbonded cutoff distance in eh NPT ensemble (after warmup). The simulation was initiated at 100 K and minimized for 1000 steps with all protein atoms held fixed. The system was then warmed to 300 K at a rate of 0.005 K/fs, and run at 300 K for 10000 steps while protein atoms remained fixed. The system was then held at 300 K, and protein atoms were restrained with a force constant of 100. The force constant was reduced at a rate of 1 per ps, until the system was allowed to run unrestrained after 0.206 ns. The simulations were run to a total of 5,000,000 timesteps (10 ns). Equilibrium was determined by observing stabilization of total system energy (E_{Tot}) and backbone RMSD. (Fig. S11)

Chromophore Geometries: HP35. As for the polyproline peptides, a Tcl script was run in VMD to determine the distance between the leucyl carbonyl and phenylanine ring at every tenth timestep over the last 9 ns of the trajectory. Again, the interchromophore distance (*R*) was determined between CEmp of Phe_{35} and the midpoint between Leu_1 C and Ser_2 N (CNmp). The time-averaged value of *R* is 19.2 Å with an RMSD of 1.8 Å.

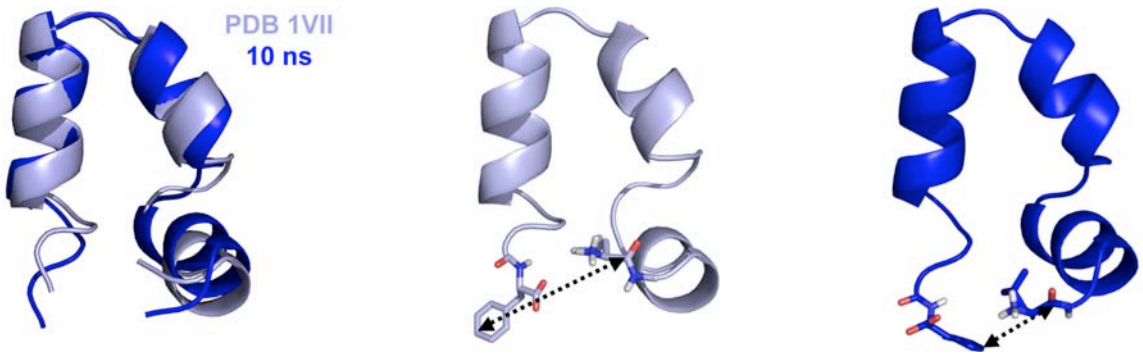

Figure S10. HP35 Structures. HP35 starting structure (PDB 1VII) shown aligned with HP35 after 10 ns of dynamics. Leu_1/Phe_{35} interaction shown with arrow. Alignment and rendering using PyMOL.

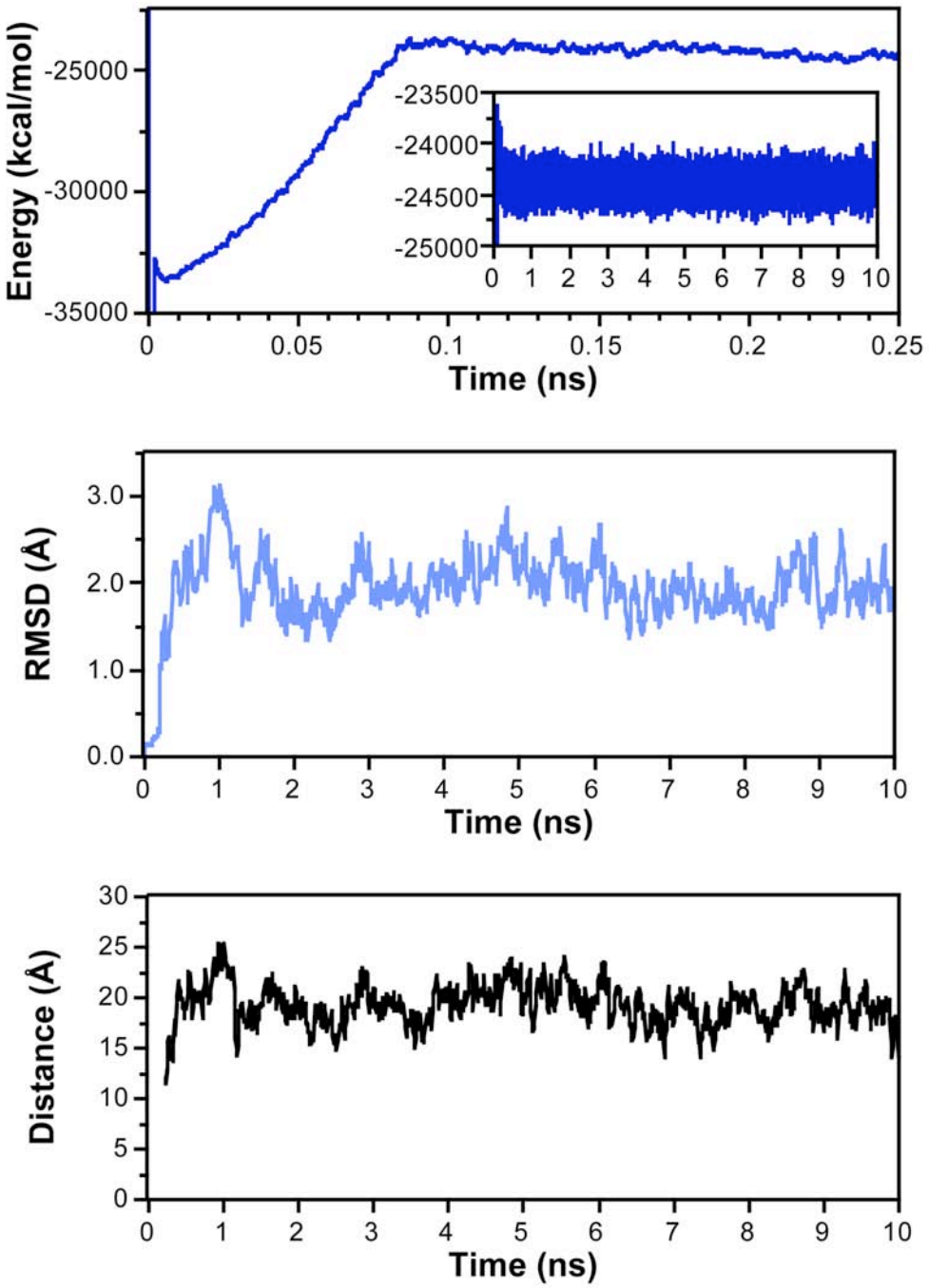

Figure S11. HP35 Trajectory Analysis. Top: Total system energy during startup phase. Inset shows entire 10 ns simulation. Middle: Backbone RMSD relative to starting structure. Bottom: L_1 carbonyl midpoint to F_{35} Cε1/Cε2 midpoint distance.

Villin HP35 Variant Circular Dichroism Measurements. Temperature-dependent circular dichroism (CD) data were obtained in phosphate buffer monitoring at 222 nm, between 5 and 95 ºC, using the variable temperature module provided with the Aviv 410 CD spectrometer. Data were collected with a 1 °C/min temperature slope, 5 s averaging time, 1 min temperature equilibration time, 5 s response time, and 1 nm band width. The resulting raw ellipticity (θ_D) measurements were transformed to molar residue ellipticity values (θ) using equation (S10).

$$\theta = \theta_D / (c l n_R) \qquad \text{(S10)}$$

where c is concentration (M), l is path length (cm), and n_R is the number of residues. To determine fraction folded (f_f) for each peptide, linear baselines were fit to the data below 20 °C ($\theta_F = m_F T + b_F$) or above 80 °C ($\theta_U = m_U T + b_U$). The full data range was then fit to equation (S11) where $K = e^{-(\Delta H - T\Delta S)/RT}$, ΔH and ΔS are adjustable parameters and R = 8.3145 J•mol^{-1}•K^{-1}.

$$\theta = \theta_F(T)(1-f_f(T)) + \theta_U(T)f_f(T) \qquad f_f = K/(1+K) \qquad \text{(S11)}$$

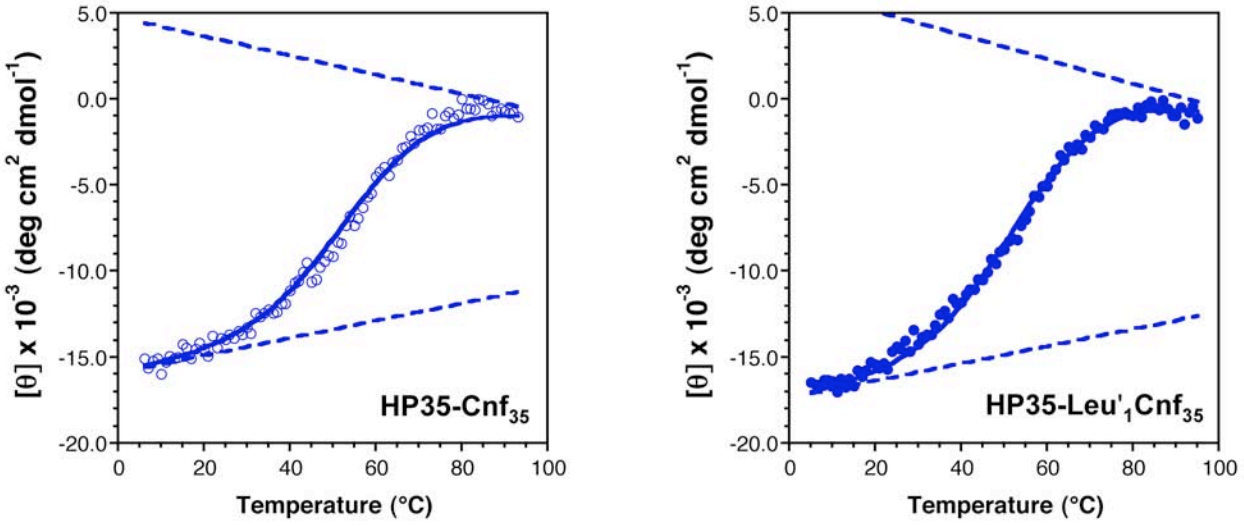

Figure S12. Temperature-Dependent Circular Dichroism Data. Molar residue ellipticity (θ) at 222 nm measured for 10 μM solutions of HP35-F*$_{35}$ (open circles) and HP35-L'$_1$F*$_{35}$ (filled circles) in phosphate buffer. Baselines are shown as dotted lines. Data are shown circles, lines indicate fit to equation S11.

HP35 Variant Temperature Dependent Fluorescence Intensity. Temperature-dependent fluorescence intensities at 293 nm were acquired for 10 μM HP35-L'$_1$F*$_{35}$ or HP35-F*$_{35}$ as described above. The data were normalized to the fluorescence intensity of HP35-F*$_{35}$ at 5 °C. Given the strong temperature dependence of Cnf fluorescence, normalization of HP35-L'$_1$F*$_{35}$ fluorescence to HP35-F*$_{35}$ is essential. E_Q was computed by taking the ratio of the fluorescence emission of HP35-L'$_1$F*$_{35}$ (F) to the emission of HP35-F*$_{35}$ (F_0) at a given temperature according to equation (S6). This was then converted to a measure of chromophore separation based on Förster theory (R_{FRET}) using equation (S12) with R_0 = 16.5 Å, the value experimentally determined for the proline series.

$$R_{FRET} = R_0\left(\frac{1}{E_Q} - 1\right)^{1/6} \qquad \text{(S12)}$$

For comparison, E_Q was also converted to a measure of chromophore separation based on Dexter theory (R_{Dex}) using equation (S13) with L_{Dex} = 7.1 Å, and k = 8.9 x 10^{-3}, the values determined by least-squares fitting of the proline series data.

$$R_{Dex} = \frac{1}{2} L_{Dex}\left[\ln\left(\frac{1 - E_Q}{kE_Q}\right)\right] \qquad \text{(S13)}$$

The resulting Leu'$_1$/Cnf*$_{35}$ chromophore separations R_{FRET} and R_{Dex} are shown in Figure S13, with R_{FRET} ranging from 20.8 Å at 5 °C to ≥ 30 Å at 75 °C and R_{Dex} ranging from 21.7 Å at 5 °C to ≥ 30 Å at 75 °C. The RMSD of R_{FRET} and R_{Dex} between 5 and 75 °C is 0.8 Å. Thus, the choice of mechanistic interpretation has relatively little impact on the interchromophore distance one extracts from the fluorescence data.

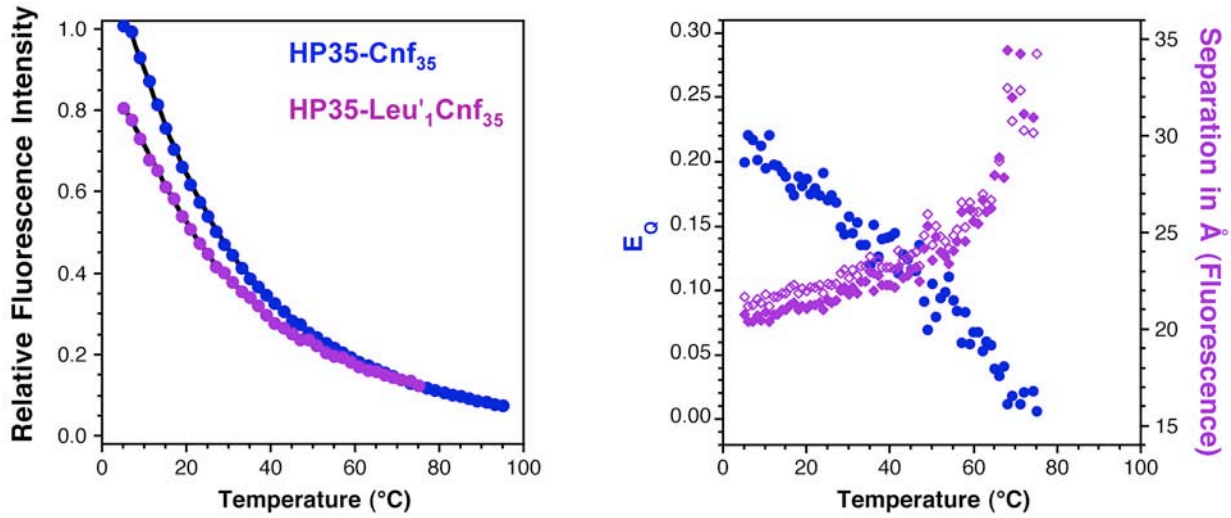

Figure S13. Temperature-Dependent Fluorescence Data. Left: Normalized fluorescence intensity at 293 nm of HP35-F*$_{35}$ and HP35-L'$_1$F*$_{35}$ in phosphate buffer. Right: E_Q computed from normalized fluorescence data (blue circles) and corresponding Leu'$_1$/Cnf$_{35}$ separation determined from E_Q using equation S12 (R_{FRET}, closed diamonds) or equation S13 (R_{Dex}, open diamonds).

References

(1) Shalaby, M. A.; Grote, C. W.; Rapoport, H. *J. Org. Chem.* **1996**, *61*, 9045-9048.

(2) Tucker, M. J.; Oyola, R.; Gai, F. *J. Phys. Chem. B* **2005**, *109*, 4788-4795.

(3) Forster, T. *Discucc. Faraday Soc.* **1959**, 7-17.

(4) Van Der Meer, B. W.; Coker III, G.; Chen, S.-Y. S. *Resonance Energy Transfer*; VCH Publishers, Inc.: New York, NY U.S.A., 1994.

(5) Helbing, J.; Bregy, H.; Bredenbeck, J.; Pfister, R.; Hamm, P.; Huber, R.; Wachtveitl, J.; De Vico, L.; Olivucci, M. *J. Am. Chem. Soc.* **2004**, *126*, 8823-8834.

(6) Tucker, M. J.; Oyola, R.; Gai, F. *Biopolymers* **2006**, *83*, 571-576.

(7) Dexter, D. L. *J. Chem. Phys.* **1953**, *21*, 836-850.

(8) Speiser, S. *Chem. Rev.* **1996**, *96*, 1953-1976.

(9) Taskent-Sezgin, H.; Marek, P.; Thomas, R.; Goldberg, D.; Chung, J.; Carrico, I.; Raleigh, D. P. *Biochemistry* **2010**, *49*, 6290-6295.

(10) Stewart, W. E.; Siddall, T. H. *Chem. Rev.* **1970**, *70*, 517-&.

(11) Frisch, M. J.; Trucks, G. W.; Schlegel, H. B.; Scuseria, G. E.; Robb, M. A.; Cheeseman, J. R.; Montgomery, J., J. A.; Vreven, T.; Kudin, K. N.; Burant, J. C.; Millam, J. M.; Iyengar, S. S.; Tomasi, J.; Barone, V.; Mennucci, B.; Cossi, M.; Scalmani, G.; Rega, N.; Petersson, G. A.; Nakatsuji, H.; Hada, M.; Ehara, M.; Toyota, K.; Fukuda, R.; Hasegawa, J.; Ishida, M.; Nakajima, T.; Honda, Y.; Kitao, O.; Nakai, H.; Klene, M.; Li, X.; Knox, J. E.; Hratchian, H. P.; Cross, J. B.; Bakken, V.; Adamo, C.; Jaramillo, J.; Gomperts, R.; Stratmann, R. E.; Yazyev, O.; Austin, A. J.; Cammi, R.; Pomelli, C.; Ochterski, J. W.; Ayala, P. Y.; Morokuma, K.; Voth, G. A.; Salvador, P.; Dannenberg, J. J.; Zakrzewski, V. G.; Dapprich, S.; Daniels, A. D.; Strain, M. C.; Farkas, O.; Malick, D. K.; Rabuck, A. D.; Raghavachari, K.; Foresman, J. B.; Ortiz, J. V.; Cui, Q.; Baboul, A. G.; Clifford, S.; Cioslowski, J.; Stefanov, B. B.; Liu, G.; Liashenko, A.; Piskorz, P.; Komaromi, I.; Martin, R. L.; Fox, D. J.; Keith, T.; Al-Laham, M. A.; Peng, C. Y.; Nanayakkara, A.; Challacombe, M.; Gill, P. M. W.; Johnson, B.; Chen, W.; Wong, M. W.; Gonzalez, C.; Pople, J. A.; Gaussian, Inc.: Pittsburgh PA, 1998.

(12) Hara, K.; Suzuki, H.; Rettig, W. *Chem. Phys. Lett.* **1988**, *145*, 269-272.

(13) Lewis, F. D.; Holman, B. *J. Phys. Chem.* **1980**, *84*, 2326-2328.

(14) Bondi, A. *J. Phys. Chem.* **1964**, *68*, 441-451.

(15) Kale, L.; Skeel, R.; Bhandarkar, M.; Brunner, R.; Gursoy, A.; Krawetz, N.; Phillips, J.; Shinozaki, A.; Varadarajan, K.; Schulten, K. *J. Comp. Phys.* **1999**, *151*, 283-312.

(16) Darden, T.; York, D.; Pedersen, L. *J. Chem. Phys.* **1993**, *98*, 10089-10092.

(17) McKnight, C. J.; Matsudaira, P. T.; Kim, P. S. *Nat. Struct. Biol.* **1997**, *4*, 180-184.